Journal of Power Sources 232 (2013) 139–151

Contents lists available at SciVerse ScienceDirect

Journal of Power Sources

journal homepage: www.elsevier.com/locate/jpowsour

A general approach to develop reduced order models for simulation of solid oxide fuel cell stacks

Wenxiao Pan*,[1], Jie Bao [1], Chaomei Lo, Kevin Lai, Khushbu Agarwal, Brian J. Koeppel, Moe Khaleel

Pacific Northwest National Laboratory, P.O. Box 999, MS-IN K7-90, Richland, WA 99352, USA

HIGHLIGHTS

- A general approach is provided to develop reduced order models.
- The approach provides rapid calculation with higher fidelity stack information.
- Response surface analysis characterizes the stack over a wide operating space.
- Accurate and efficient response surface generation is based on sensitivity and error analyses.
- Principal component analysis is used to reduce order of state variables.

ARTICLE INFO

Article history:
Received 13 October 2012
Received in revised form
26 December 2012
Accepted 11 January 2013
Available online 17 January 2013

Keywords:
Solid oxide fuel cell
Reduced order modeling
System modeling
Mathematical modeling
Sensitivity analysis
Responsive surface

ABSTRACT

Numerical models for solid oxide fuel cells (SOFCs) are needed in system modeling studies of fuel cell-based power generation systems. A reduced order modeling approach based on response surface techniques is developed for SOFC stacks. This approach creates a numerical model that can quickly compute desired performance variables of interest based on the stack's input parameter state. The developed method first carefully samples the multidimensional design space based on the input parameter ranges, automatically evaluates an existing detailed stack model at each of the sampled points, and performs regression for selected performance variables of interest to determine the response surfaces. After error analysis to ensure that sufficient accuracy is established for the response surfaces, they are then implemented in a calculator module for use by the system-level software. The benefit of this modeling approach is that it is sufficiently fast for integration with system modeling software while still providing high fidelity information about the internal distributions of key variables in the fuel cell. This paper describes the sampling, regression, sensitivity, error, and principal component analysis to identify the most appropriate methods for simulating a planar SOFC stack.

© 2013 Elsevier B.V. All rights reserved.

1. Introduction

The solid oxide fuel cell (SOFC) is a highly desirable energy conversion device [1] due to its high efficiency, high power density, fuel flexibility, ability to support on-cell reformation, low emissions, and production of byproduct heat for cogeneration. Active research is in progress to use the SOFC for large-scale power generation [2,3], as well as distributed generation [4] and even portable transportation applications [5]. A complete fuel cell system requires various hardware components (e.g. blowers, heat exchangers, reactors, combustors, compressors, etc.) that must be carefully integrated for high overall efficiency, so system modeling is critical to define new, cost-efficient plant designs that take advantage of the SOFC's unique features.

These system models must include a mathematical submodel that represents the performance and response of the fuel cell stack, but the submodels used to represent the stack in system analyses typically are only non-dimensional thermodynamic models with a simple mass and energy balance for the entire stack structure. They can compute the stack voltage as a function of single average stack temperature and fuel utilization, but they ignore the influence of any internal distributions. This coarse level of detail is usually selected for its computational speed, as the system model requires many iterations to converge to a steady-state solution or to compute transient changes in dynamic simulations. A fully detailed calculation with stack distributions for species, current density, and temperature usually is too computationally expensive to be used. However, it is

* Corresponding author. Tel.: +1 509 375 6686; fax: +1 509 372 4720.
E-mail address: wenxiao.pan@pnnl.gov (W. Pan).
[1] Equal contribution.

0378-7753/$ – see front matter © 2013 Elsevier B.V. All rights reserved.
http://dx.doi.org/10.1016/j.jpowsour.2013.01.057

well known that temperature and current density gradients exist within large stacks [6]. These gradients have important effects on the electrochemical performance, but, perhaps more significantly, the upper and lower temperatures of the cells are not captured. The upper temperature limit usually is a critical design parameter to prevent excessive degradation from thermally activated mechanisms, such as oxide scale growth on the metallic interconnect. The lower temperature limit is important because reduced ionic conductivity of the electrolyte results in poor electrochemical performance that decreases the working voltage of the planar cells. Therefore, models that attempt to capture the distributions within the stack are of high interest [7], and neglecting these dimensional effects can lead to inaccuracy, such as overestimation of the system efficiency [8]. Therefore, a method that provides high fidelity data about the stack distributions with minimal runtime computations is needed to accurately characterize the SOFC operating state in system studies.

While the SOFC conventionally uses H_2 as its fuel, it can also utilize carbon-based fuels that contain CH_4. The high operating temperature of the SOFC and availability of steam from the H_2 oxidation reaction permits direct internal steam reformation of CH_4 to H_2 on the Ni particles of the cermet anode. This endothermic reformation reaction in the SOFC can be judiciously used for thermal management of large stacks by reducing high temperatures, but inadequate control of spatial reformation on the cell can result in excessive local cooling that can create thermal–mechanical stresses or reduced electrochemical activity. Presently in the U.S., natural gas (whose composition can contain 70–90% CH_4) is abundant and inexpensive due to enhanced recovery techniques from shale deposits. Based on continued development of shale resources, the U.S. natural gas supply is expected to grow over the next two decades, and the country is predicted to become a net exporter by 2022 [9]. Low prices, combined with potential cooling benefits, could make natural gas a highly attractive feedstock for future electric power generation. Therefore, the developed SOFC modeling tools should demonstrate the capability to analyze conventional H_2 fuels as well as reforming compositions containing CH_4.

Numerical simulations for complex systems, such as power generation plants, need to be computationally tractable for general use by the designer; therefore, considerable attention has been paid to reducing the computational cost by developing reduced order models (ROMs) [10–15]. In recent years, reduced order modeling techniques have proven to be powerful tools for various problems, such as circuit design [16,17], software development efforts [18], activation of bacteria [19], aircraft design [20,21], etc. A suitable ROM that closely approximates the high-fidelity SOFC stack models and accounts for internal temperature distributions will be a valuable tool toward improving the accuracy of system simulations that are essential to development and planning for future large-scale, fuel cell-based power plants.

Generally, the problem of model reduction is to replace a given mathematical model of a system or process by a model that is much "smaller" or "simpler" than the original—but still describes, at least, certain aspects of the system or process approximately. Hence, ROMs usually are thought of as computationally inexpensive models that can offer the potential for near real-time analysis [10]. However, ROM construction often is considered as time-consumable and computationally expensive because it requires accumulating a large number of system responses to input excitations [20]. Therefore, an efficient sampling method, sensitivity analysis of input factors and their ranges, and an appropriate regression method are critical to the efficiency and accuracy of the ROM.

The present study proposes a general approach to develop the ROM for simulating SOFC stacks in an efficient manner. In particular, through a sensitivity analysis, we rank the input variables according to their contributions to the sensitivity of each output quantity (see Section 3). The responsive relations are established between the outputs of interest and the inputs through appropriate regression methods (see Section 4). Furthermore, using a recently developed multi-element probabilistic collocation (ME-PCM) method, the distribution of sensitivity is accurately quantified in different regions of input parameter space (see Section 5). Finally, based on the principal component analysis (PCA), outputs with special distributions (i.e., state variables) can be predicted, e.g. temperature distributions within each cell, by establishing an efficient mapping from inputs to their ranked scores (see Section 6). In order to clearly demonstrate the application of the ROM tool to study the SOFC, the proposed approach is mainly applied to a baseline H_2-fueled stack using a previously published quasi-two-dimensional electrochemistry model for planar SOFC stacks [6]. The endothermic steam reforming reaction of a CH_4 fuel introduces much more complexity to the thermal response of the model, so thorough analysis of reforming fuel compositions and cases will not be presented in this paper. Rather, a fuel composition with CH_4 was used with the same model [6] to briefly compare the effect of an alternate reforming fuel composition on the sensitivity analysis.

2. SOFC model description

2.1. Detailed stack electrochemistry model

A numerical model, called SOFC-MP 2D, was previously developed to simulate the performance of tall SOFC stacks [6]. For symmetric co-flow or counter-flow planar cells where the lateral variations of species, current, and temperature are sufficiently small, a reasonable approach is to consider only the distributions along the flow channel direction and between each series-connected cell. This provides a useful but computationally efficient approach to analyze tall stack towers where significant thermal gradients will develop. This numerical model was used as the demonstration input model for the ROM creation exercise.

The SOFC-MP 2D numerical model consists of an arbitrary number of planar cells composed of the anode-electrolyte-cathode tri-layer, air channel, fuel channel, and interconnect structure. The electrochemical model consists of a one-dimensional approximation applied at each computational point on the iso-potential cell that accounts for the activation, concentration, and ohmic losses based on the local temperature and species concentrations. The flow model solves the species balances for the fuel and oxidant streams, while the thermal model solves the energy balance for the solid and fluid domains, considering conduction, convection, and radiation heat transfer mechanisms. The steady-state results distributions for fuel species, oxidant species, current, and temperature in every cell are calculated, as well as global stack performance metrics, such as current, power, utilizations, peak temperatures, outlet temperatures, etc. For this demonstration model, we focus on a 97% H_2 fuel composition, with a 625 cm^2 16-cell stack in a 750 °C furnace environment (denoted as the H_2 case for short). For investigating the effect of different fuel composition on sensitivity analysis, a fuel with CH_4 was used as well, which contains 11% CH_4, 32.4% H_2, 33.3% H_2O, 4.9% CO, 6.1% CO_2, and 12.4% N_2 (denoted as the CH_4 case for short). The CH_4 case was tested in the same cell/stack design as the H_2 case. The CH_4 case is only used in the input parameter sensitivity analysis as a comparison to the H_2 case; all of the remaining analyses (regression for response surface, sensitivity of region of inputs, and prediction of state variables by principle component analysis) are based on the H_2 case simulation results.

2.2. Input and output parameters

In the demonstration case, four input parameters and five output parameters were selected for studying the impact of different factors that affect the fuel cell's performance. The inputs include the stack fuel flow rate, stack voltage, stack oxidant flow rate, and fuel temperature. Table 1 lists the input ranges. To ensure that the average stack temperature is high enough for good electrolyte conductivity and cell performance, the minimum fuel temperature for the CH_4 case was increased from 650 to 700 °C as shown in Table 1. To reduce the order of the input parameters in the development model, the inlet fuel and oxidant temperature were assumed to be the same. The output variables of interest are stack current, cell maximum temperature, outlet fuel temperature, outlet fuel H_2 molar fraction, and outlet oxidant temperature.

3. Sensitivity analysis

3.1. Methods for sensitivity analysis

We first demonstrate the input variables that most contribute to overall global sensitivity are determined by studying the contribution of each input variable to the sensitivity of outputs. From the fuel cell designer's perspective, this information identifies the operational parameters wherein stack performance is very sensitive and appropriate controls are necessary for stable operation in an integrated power system. Three methods are used to rank the contribution of input parameters. The first is calculating the absolute value of standardized regression coefficients (SRCs) as a measure of variable importance. The second is the analysis of variance or deviance (ANOVA) based method, which uses the value of the residual of deviance in the generalized linear method (GLM) as a quantitative measurement. The third is the multivariate adaptive regression splines (MARS) based sensitivity analysis. The algorithm of each method is explained specifically in the following section.

3.1.1. Absolute value of SRCs

A linear polynomial regression analysis assumes the following form:

$$Y_m = \sum_{k=1}^{n} b_k x_k^m + b_0 + \varepsilon_m. \tag{1}$$

For the m-th sample points, x are the input parameters, b are the coefficients to be determined, Y is the output from the computational model, and ε is the discrepancy between the simulation model output and the regression results. For the k-th input parameter, the SRC is defined as [22–24]:

$$\mathrm{SRC} = \frac{b_k \widehat{s}_k}{\widehat{s}}, \tag{2}$$

Table 1
Input parameters and their predefined ranges.

Input parameters	Range
Stack fuel flow rate	0.04–0.06 mol s^{-1}
Stack voltage	11.5–13.7 V
Stack oxidant flow rate	0.206–0.6 mol s^{-1}
Fuel temperature	650–750 °C for H_2 case, 700–750 °C for CH_4 case

where

$$\widehat{s} = \left[\frac{1}{M-1}\sum_{m=1}^{M}\left(Y_m - \overline{Y}\right)^2\right]^{1/2} \text{ and } \widehat{s}_k = \left[\frac{1}{M-1}\sum_{m=1}^{M}\left(x_k^m - \overline{x}_k\right)^2\right]^{1/2}. \tag{3}$$

and M is the total number of sampling sets. A second-order polynomial regression analysis assumes the form as Eq. (4), which considered the second-order interaction terms:

$$Y_m = \sum_{k=1}^{n}\sum_{j\le k}^{n} b_{kj} x_k^m x_j^m + \sum_{k=1}^{n} b_k x_k^m + b_0 + \varepsilon_m. \tag{4}$$

For the second-order terms, the SRC can be calculated by a similar approach, and they are:

$$\mathrm{SRC} = \frac{b_{kj}\widehat{s}_{kj}}{\widehat{s}}, \tag{5}$$

where

$$\widehat{s}_{kj} = \left[\frac{1}{M-1}\sum_{m=1}^{M}\left(x_k^m - \overline{x}_k\right)^2\right]^{1/2}\left[\frac{1}{M-1}\sum_{m=1}^{M}\left(x_j^m - \overline{x}_j\right)^2\right]^{1/2}. \tag{6}$$

A third-order polynomial regression analysis assumes the form as Eq. (7), and the SRCs for third-order terms are calculated by Eqs. (8) and (9):

$$Y_m = \sum_{k=1}^{n}\sum_{j\le k}^{n}\sum_{i\le j}^{n} b_{kji} x_k^m x_j^m x_i^m + \sum_{k=1}^{n}\sum_{j\le k}^{n} b_{kj} x_k^m x_j^m + \sum_{k=1}^{n} b_k x_k^m + b_0 + \varepsilon_m. \tag{7}$$

$$\mathrm{SRC} = \frac{b_{kj}\widehat{s}_{kji}}{\widehat{s}}, \tag{8}$$

where

$$\widehat{s}_{kji} = \left[\frac{1}{M-1}\sum_{m=1}^{M}\left(x_k^m - \overline{x}_k\right)^2\right]^{1/2}\left[\frac{1}{M-1}\sum_{m=1}^{M}\left(x_j^m - \overline{x}_j\right)^2\right]^{1/2} \times \left[\frac{1}{M-1}\sum_{m=1}^{M}\left(x_i^m - \overline{x}_i\right)^2\right]^{1/2}. \tag{9}$$

The absolute value of SRCs can be considered as a quantitative criterion for measuring the importance of each term. The larger the absolute value of the SRC, the more important its corresponding input parameter is to the sensitivity of outputs.

3.1.2. Analysis of variance based method

The GLM regression analysis with the second-order interaction terms assumes the following form [25]:

$$Y_m = \sum_{k=1}^{n} b_k x_k^m + \sum_{k=1}^{n}\sum_{j<k}^{n} b_{kj} x_k^m x_j^m + b_0 + \varepsilon_m. \tag{10}$$

The residual of deviance (RD) of the fitting system for adding each variable can be calculated by [26,27]:

$$
\begin{aligned}
\mathrm{RD}(b_0) &= \mathrm{var}(Y) - \mathrm{var}(b_0) = \mathrm{var}(Y),\\
\mathrm{RD}(x_1) &= \mathrm{var}(Y) - \mathrm{var}(b_1x_1 + b_0),\\
\mathrm{RD}(x_2) &= \mathrm{var}(Y) - \mathrm{var}(b_1x_1 + b_2x_2 + b_0),\\
\mathrm{RD}(x_3) &= \mathrm{var}(Y) - \mathrm{var}(b_1x_1 + b_2x_2 + b_3x_3 + b_0),\\
&\vdots\\
\mathrm{RD}(x_n) &= \mathrm{var}(Y) - \mathrm{var}(b_1x_1 + b_2x_2 + \cdots + b_nx_n + b_0),\\
\mathrm{RD}(x_1x_2) &= \mathrm{var}(Y) - \mathrm{var}(b_1x_1 + b_2x_2 + \cdots + b_nx_n + b_{12}x_1x_2 + b_0),\\
\mathrm{RD}(x_1x_3) &= \mathrm{var}(Y) - \mathrm{var}(b_1x_1 + b_2x_2 + \cdots + b_nx_n + b_{12}x_1x_2 + b_{13}x_1x_3 + b_0),\\
&\vdots\\
\mathrm{RD}(x_{n-2}x_n) &= \mathrm{var}(Y) - \mathrm{var}\left(b_1x_1 + \cdots + b_nx_n + b_{12}x_1x_2 + \cdots + b_{n-2,n}x_{n-2}x_n + b_0\right),\\
\mathrm{RD}(x_{n-1}x_n) &= \mathrm{var}(Y) - \mathrm{var}\left(b_1x_1 + \cdots + b_nx_n + b_{12}x_1x_2 + \cdots + b_{n-1,n}x_{n-1}x_n + b_0\right).
\end{aligned}
\tag{11}
$$

The contribution of input x_1 for the fitting system is [28]:

$$C(x_1) = \mathrm{RD}(b_0) - \mathrm{RD}(x_1), \tag{12}$$

and the contribution of x_2 is $C(x_2) = \mathrm{RD}(x_1) - \mathrm{RD}(x_2)$. Similarly, the contribution of x_n is $C(x_n) = \mathrm{RD}(x_{n-1}) - \mathrm{RD}(x_n)$. For the second-order interaction terms, the contribution of $x_{n-1}x_n$ is $C(x_{n-1}x_n) = \mathrm{RD}(x_{n-2}x_n) - \mathrm{RD}(x_{n-1}x_n)$. The calculated contribution of each term then is ranked to evaluate the relative importance of input parameters to the sensitivity of outputs. Analysis of the variance based method is not only available for the GLM regression method, but it also can be used for other regression methods, such as higher order polynomial regression.

3.1.3. MARS based sensitivity analysis

The approximation of MARS takes the form of an expansion in multivariate spline basis functions:

$$\widehat{f}(x_1, \cdots, x_n) = \sum_{m=0}^{M} a_m B_m(x_1, \cdots, x_n) \tag{13}$$

with:

$$B_0(x_1, \cdots, x_n) = 1 \tag{14}$$

$$B_m(x_1, \cdots, x_n) = \prod_{k=1}^{K_m} b\left(x_{v(k,m)} \middle| t_{km}\right), \quad m \geq 1. \tag{15}$$

The n is the number of input parameters, and M is the number of expansion terms. The details for definition and calculation of the coefficients and variables in Eq. (13)–(15) are introduced in Friedman's work [29–32]. The sensitivity analysis is based on generalized cross-validation (GCV) criterion [33,34]:

$$\mathrm{GCV}(M) = \frac{1}{N}\sum_{i=1}^{N}\left[y_i - \widehat{f}_M(x_{1i}, \cdots, x_{ni})\right]^2 \Big/ \left[1 - \frac{C(M)}{N}\right]^2, \tag{16}$$

where N is the number of simulation or experiment trials, y_i are output parameters of trials, and:

$$C(M) = (d+1)M + 1. \tag{17}$$

The recommended value of d is 2 [33]. To examine the importance of each input parameter, the parameters can be removed one by one from Eq. (16), and the increase of GCV after removing each input can be considered as the impact of the corresponding input parameter. The larger the increase of GCV after removing the certain input parameter, the more contribution of the corresponding input parameter to the system.

3.2. Results for sensitivity analysis

3.2.1. Sampling points of input parameters

Because sensitivity analysis is based on multiple simulation trial cases for different values of input parameters, sampling points should be generated uniformly in the whole range of the parameters without introducing bias. However, as the model's dimension is increased, the number of sampling points required by a systematic approach to adequately cover the model space becomes unreasonable. Thus, random or pseudorandom means must be incorporated. Over the last two decades, the quasi-Monte Carlo (QMC) method has become an increasingly popular sampling method because of its faster convergence and effective sampling of high-dimension parameter space without clumping [35,36]. To develop reliable response between the output and input parameters, it was found that in the example four-dimensional input space, 128 samples are adequate for a reliable analysis. The paired scatter plot of the sampling points generated by QMC for the four independent input parameters is shown in Fig. 1.

3.2.2. Ranking of input parameters

Fig. 2 shows the boxplot [37–39] of the 128 sampling points for the four input parameters and their corresponding five outputs for the H_2 case. It only illustrates the dependence of outputs on different inputs qualitatively. However, the three methods already introduced provide ways to examine the significance of each input quantitatively. To make the sensitivity measurements comparable between different approaches, the importance indicators in different analysis methods are scaled to scores between 0 and 100, i.e., the score of the most important factor is always normalized to be 100.

Figs. 3–7 show the important scores for the H_2 case of input parameters for each output, respectively. Because the impacts of interaction terms of the second and higher order are significantly low for this case, i.e., their scores are close to 0, they are not displayed in these figures. The three methods show the same rank for the four input factors. Notably, the sensitivity analysis based on MARS and linear regression give especially close score values. As shown in Fig. 3, the stack current depends most strongly on the voltage, as expected. The fuel flow rate is the next significant contributor as this affects fuel utilization and the cell's Nernst voltage. The oxidant flow rate and fuel inlet temperature have a thermal effect on the cell, but the impact on current generation is relatively small compared to the other two variables. As shown in Fig. 4, the maximum cell temperature depends primarily on the current, which defines the amount of electrochemical heat generated, and the oxidant flow rate as a low air utilization is used for stack thermal management. The inlet fuel state is less significant for this case because the flow rate is considerably smaller than the air,

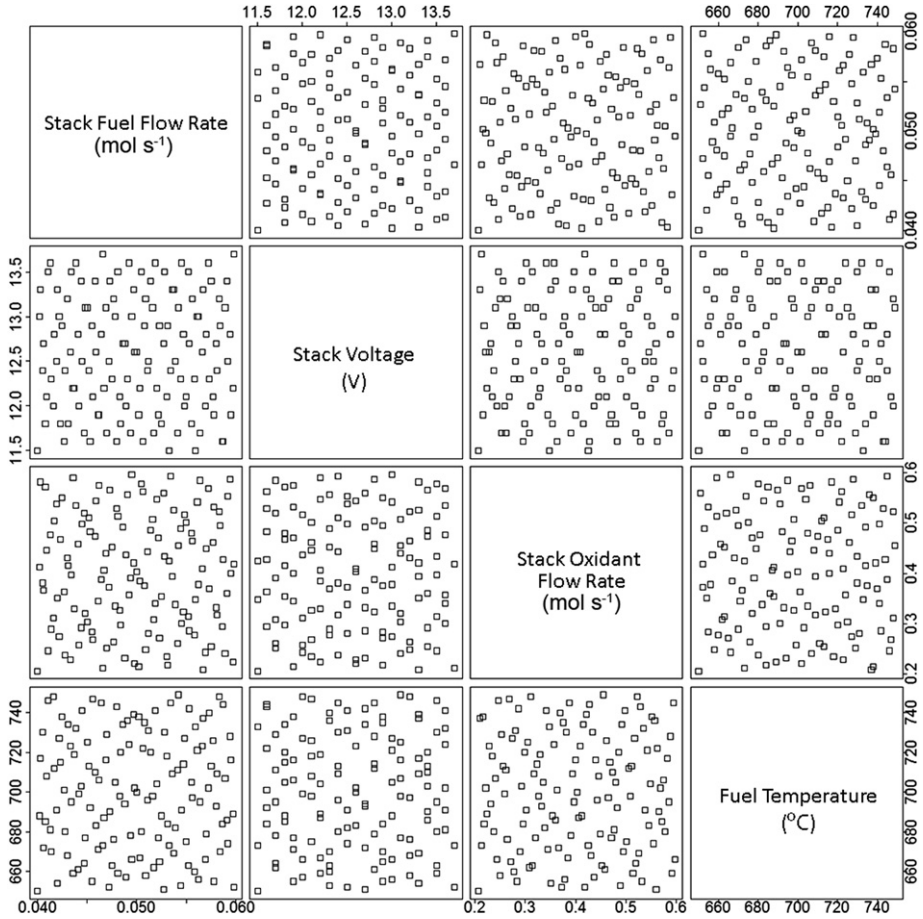

Fig. 1. Paired scatter plot of the QMC sampling points of the four independent input parameters.

resulting in less convective cooling. In Fig. 5, the outlet fuel temperature again depends more strongly on the electrochemical heat generated, oxidant convective cooling, and fuel initial temperature than the fuel rate. Fuel utilization is known based on the stack current, so the strong dependence of outlet fuel composition on stack voltage shown in Fig. 6 also is expected. The outlet oxidant temperature has a significant dependence on all of the inputs as shown in Fig. 7. The stack voltage and fuel flow rate have the largest impact by defining the total electrochemical heat generated in the cell. The oxidant flow rate has the next largest impact because it is the primary mechanism for heat removal in the stack. Finally, the fuel inlet temperature has the least thermal impact on the overall cell temperature as it has a much lower flow rate relative to the oxidant. Therefore, the sensitivity analysis replicates the expected stack behaviors for this simple case, and it will be even more insightful when an increased number of parameters are considered in more complex cases.

The same sensitivity analysis was also applied the CH_4 case to briefly investigate the effects of fuel composition on the importance scores (the input parameter sampling range is different for inlet fuel temperature as mentioned in Section 2.2). Figs. 8–12 shows the importance scores of input parameters for each output by sensitivity analysis based on MARS regression, respectively. The comparison between CH_4 and H_2 cases are shown in Figs. 8–12 as well. For the stack current, cell maximum temperature, and outlet H_2, the sensitivity ranks are the same for both CH_4 and H_2 cases, though the scores are different, as shown in Figs. 8, 9 and 11. For outlet fuel temperature in the CH_4 case, the sensitivity of fuel temperature, stack oxidant flow rate and stack fuel flow rate decrease compared to the dominant input parameter stack voltage. Also, fuel temperature becomes slightly more important than stack oxidant flow rate in the CH_4 case, as shown in Fig. 10. For outlet oxidant temperature, the second most important input parameter stack fuel flow rate in the H_2 case becomes the least important input in the CH_4 case, as shown in Fig. 12. These differing sensitivities result from interactions between the endothermic steam reformation reaction, the temperature-dependent reforming rate of the CH_4, and the temperature-dependent electrochemical performance. While the H_2 oxidation always releases heat to increase cell temperature and improve electrochemical performance, the CH_4 reformation simultaneously cools the cell resulting in poorer performance and slower reformation kinetics. Furthermore, complete reformation of the CH_4 content is achieved on the hot cell independent of the actual current as long as sufficient steam is present. The competition between these thermal mechanisms then makes the flow and temperature parameters more influential relative to the stack voltage parameter. Since cell operation with CH_4 compositions is more complex, thorough treatment of reforming fuels cannot be adequately investigated with this single case. For more precise evaluation of the impact of the fuel component fraction variation on the output parameters, more input parameters can be added into the sampling space by considering different fractions for each component within a desired range instead of the fixed composition. The same method and steps as introduced in this manuscript can be used to quantitatively score the importance of each component. Because this manuscript focuses on the method and model introduction, a complete reforming fuel component sensitivity analysis is not shown in this paper.

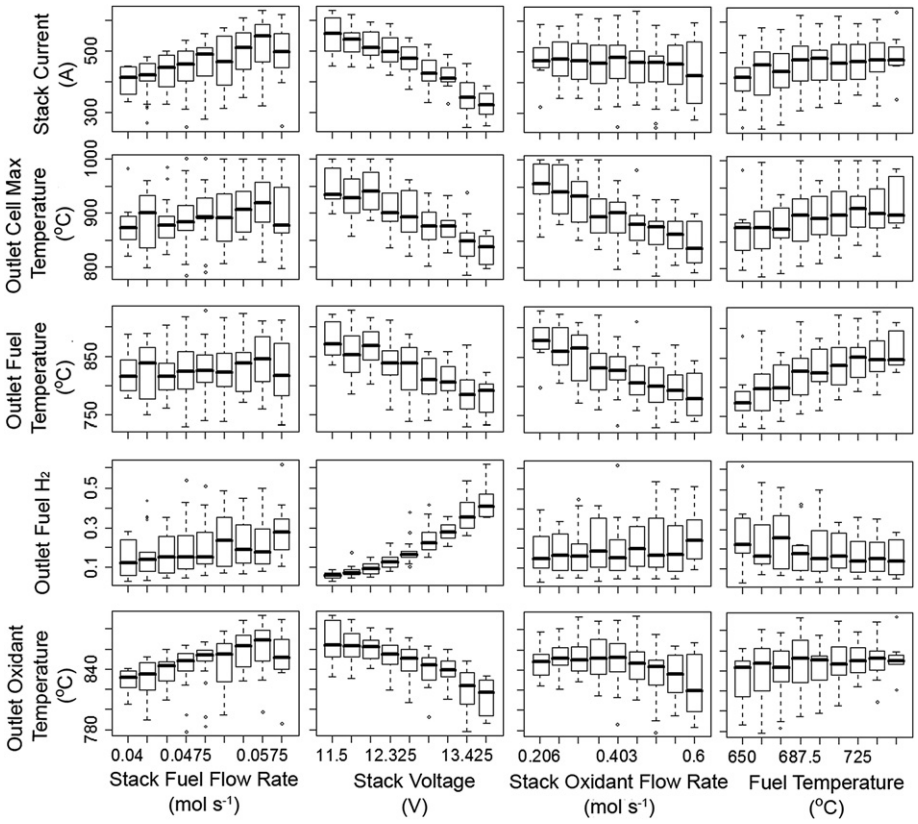

Fig. 2. Boxplot of the dependence of the five output parameters on the four input parameters.

4. Responsive relations between inputs and outputs by regression

Five regression methods are used to generate the responsive relation between the input and output variables. They are MARS, GLM, second- and third-order polynomial, and support vector regression (SVR) methods. MARS is a nonparametric regression technique and can be seen as an extension of linear models that automatically models nonlinearities and interactions between variables [40]. GLM is a flexible generalization of ordinary linear regression that allows for response variables that have distributions other than a normal distribution. Eq. (10) shows its general form, and the parameters b are calculated through the least squares method. Quadratic and cubic polynomial regressions have the same form as Eqs. (4) and (7). The parameters b also are calculated from the least squares method. SVR is developed from the support vector machines (SVM). The basic idea is to find a function that has the most deviation from the actually obtained outputs for all the training data and, at the same time, is as flat as possible [41,42]. For a linear function in the form of:

$$Y = F(X) = a^T X + b, \tag{18}$$

where a is the weighting vector and b is a translation vector. The formulated SVM approximation is: minimizing $1/2|a|^2$

$$\text{subject to } \begin{cases} Y_i - a^T X - b \le \varepsilon \\ a^T X + b - Y_i \le \varepsilon, \end{cases} \tag{19}$$

where ε is the required most deviation. Because the SVM assumption may not be realistic in general, slack variable is used to control the tradeoff between flatness and how much deviation is tolerated. Vector a can be calculated from the optimization problem (Eq. (19)), and the b vector can be calculated by using Karush–Kuhn–Tucker (KKT) conditions [43]. More details regarding SVR can be found in refs. [41–43].

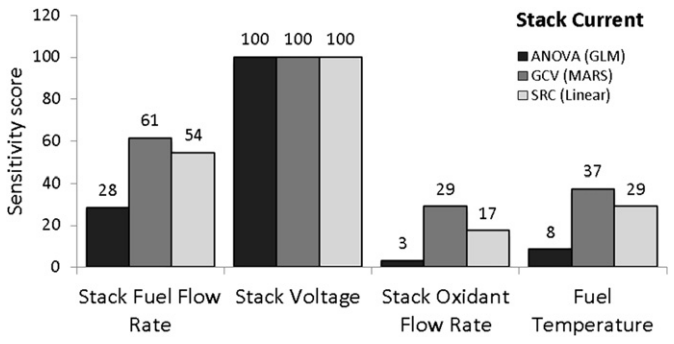

Fig. 3. Sensitivity score of input parameters for stack current.

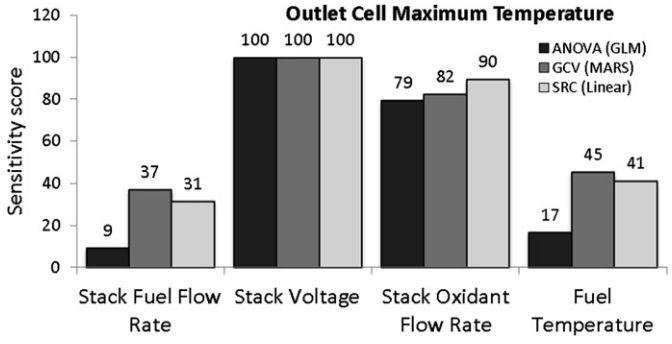

Fig. 4. Sensitivity score of input parameters for cell maximum temperature.

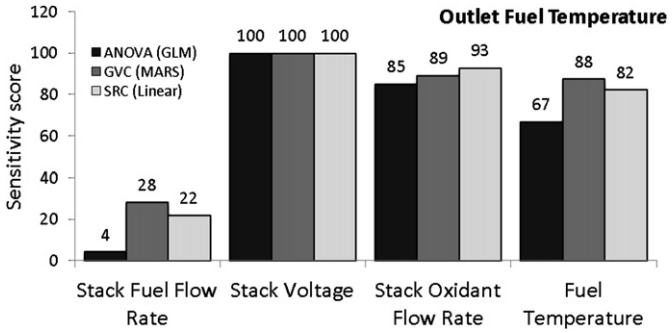

Fig. 5. Sensitivity score of input parameters for outlet fuel temperature.

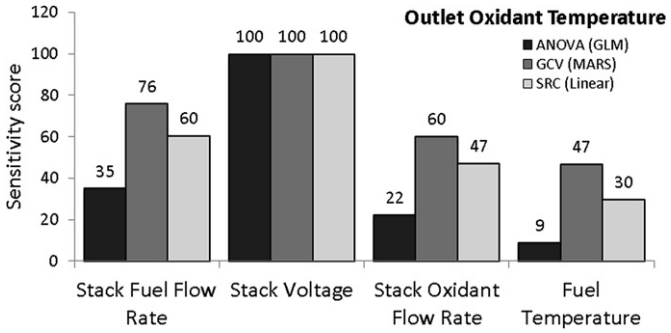

Fig. 7. Sensitivity score of input parameters for outlet oxidant temperature.

The same QMC 128 sampling points generated with the stack model in Section 3.2.1 are used as the training set. To examine the accuracy of different regression methods, another 128 sampling points in the four-dimension input space are generated as the testing set, and no duplicate points exist among the training and testing sets. As illustrative examples, only the regression results for the stack current and outlet oxidant temperature for the H_2 case are shown in Figs. 13 and 14, respectively (results for other output variables are shown in Figs. 1–3 in Supplementary data). Here, Figs. 13 and 14 (*left column*) show the correlation between the interpolated values from the training set and the actual simulation values from the testing set. In these figures, the interpolated values are named "predicted value", and the actual simulation values on the sampling points are called "actual value". If the scatter points are closer to the ideal line (solid black line in figures), the predicted value is closer to the actual value, which means the regression method is more accurate. The histograms of the scaled error (i.e. (actual − predicted)/actual) of predicted values in each regression method are also shown in Figs. 13 and 14 (*right column*). An accurate prediction should have the error distributing narrowly near the origin. As shown in Fig. 14, the error of cubic regression on all testing points is within ±0.4%. On the contrary, for a less accurate prediction, the error distribution spreads widely around the origin. As shown in Fig. 13, the GLM regression method generates the error on most testing points over ±2% which makes it unsuitable for this fuel cell model. Overall, it shows that for the investigated responsive relations of outputs to inputs in the present work, the MARS and cubic polynomial regression methods provide more accurate predictions for all five output variables. Table 2 shows the R-square value of each regression method for different output parameters, and the largest R-square values are highlighted. It is found that among the five methods for four of the outputs, the cubic polynomial regression method generates the most accurate predictions, and the MARS regression method shows the best performance for the other output, i.e., the outlet cell maximum temperature. It is consistent with the conclusion based on results shown in Figs. 13 and 14, as well as Figs. 1–3 shown in the Supplementary data.

Based on the preceding analysis, the cubic polynomial and MARS regression methods are chosen to build the responsive surfaces in the demonstration case. As an example, we calculate the responsive surface for two outputs: the stack current and outlet oxidant temperature. Because the stack fuel flow rate and stack voltage are the top two inputs in the rank for the selected two outputs (see Figs. 3 and 7), the responsive surface is calculated in the two-dimensional input space composed of these two inputs. Their range is kept as the original desired range shown in Table 1. For the other two input parameters, the stack oxidant flow rate is fixed at 0.3 mol s^{-1}, and the fuel temperature is fixed at 700 °C. To examine the responsive surface accuracy, 32 × 32 uniform distributed mesh points are generated. The actual simulation results on these 32 × 32 grids are used as the actual value to evaluate the error of the predicted value on the responsive surface that is calculated by the cubic and MARS regression methods, respectively. Fig. 15 shows the calculated responsive surface and the absolute value of scaled error (i.e., (actual − predicted)/actual)) distribution on the surface. The error in the response surface is less than 0.3% over most of the design space and no more than 4% on the edges of the domain. In addition, Table 3 shows the calculated R-square of the correlation between the predicted values and actual values on the 32 × 32 grid points. We find accurate prediction of the responsive surface using both methods. This confirms that fast computations using the developed response surfaces can acceptably represent the stack in system models.

5. Sensitivity of inputs in different regions of responsive surface by the ME-PCM

Next, a general stochastic method, called the multi-element probabilistic collocation method (ME-PCM) [44,45], is adopted for

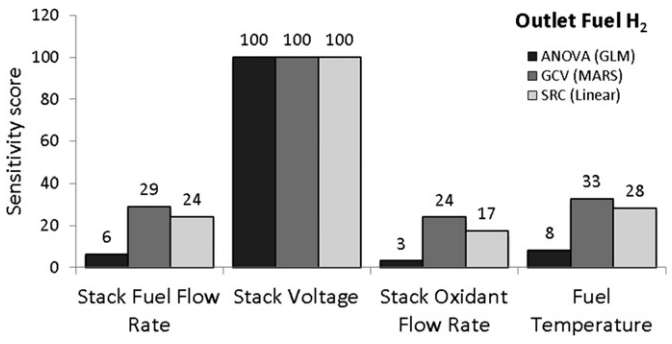

Fig. 6. Sensitivity score of input parameters for outlet fuel H_2 concentration.

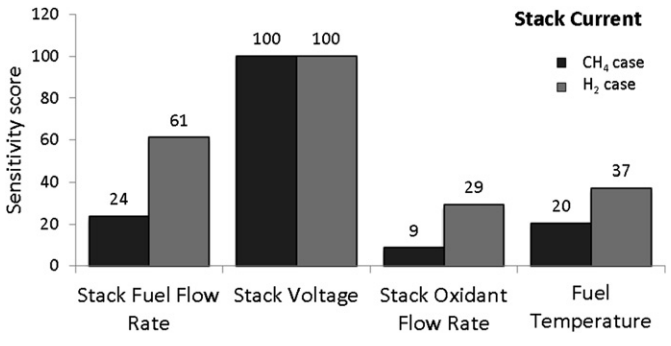

Fig. 8. Comparison of sensitivity score of input parameters between CH_4 case and H_2 case for stack current.

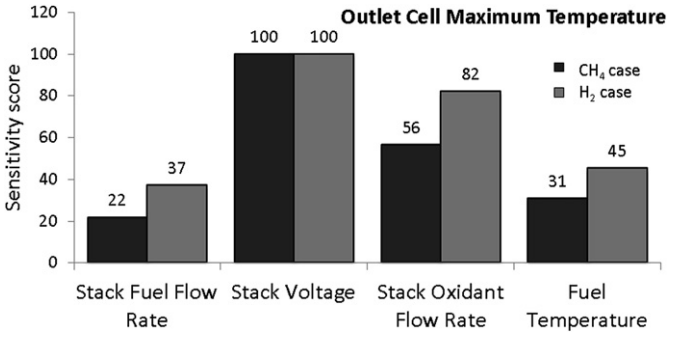

Fig. 9. Comparison of sensitivity score of input parameters between CH_4 case and H_2 case for outlet cell maximum temperature.

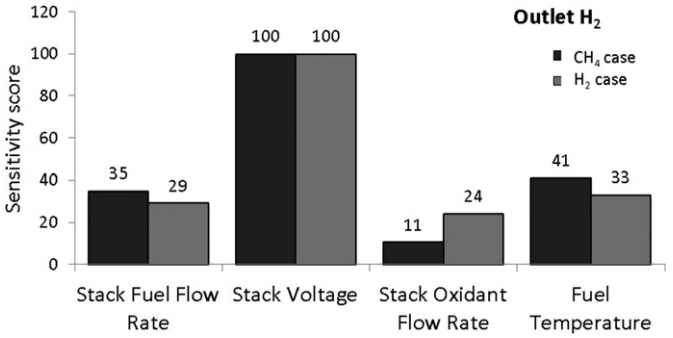

Fig. 11. Comparison of sensitivity score of input parameters between CH_4 case and H_2 case for outlet H_2.

sensitivity analysis of inputs in different regions of the response surface. The ME-PCM is based on stochastic spectral methods, a class of numerical methods widely used in engineering applications [46–48]. In the ME-PCM, input parameters are taken as stochastic quantities in the system, and output sensitivity is measured in terms of local statistical moments in multidimensional subregions of the parametric space. Local variances of the system output provide novel information about the spread of the system outcomes due to simultaneous input parameter variation throughout each subregion. If the variance is low, the system is robust to changes in this input parameter subregion. Otherwise, the system is highly sensitive in this region, perhaps indicating that further experimental efforts should be focused in this area. The ME-PCM's inherent generality allows it to be used to calculate the sensitivity of a large variety of relevant input quantities and to locate regions of high sensitivity within the parameter space. The ME-PCM also has been shown to be much more computationally efficient than Monte Carlo due to a "smart" choice of sampling points [44].

5.1. A review of the ME-PCM method

The ME-PCM uses domain decomposition and numerical quadrature rules to sample more efficiently. The sensitivity is studied for input variables within defined ranges. Each input variable x_i is assumed to vary on an interval $[a_i, b_i]$, and $\Gamma = \prod_i^n [a_i, b_i]$ is defined to be the input parameter space where n is the parameter space dimension. The ME-PCM procedure is reviewed in three steps. During the preprocessing step, the parameter space is discretized, and a set of sampling points is chosen. Next, a mathematical metric is chosen to characterize the relevant input quantities. In the last step, the sensitivity of these quantities is evaluated in each subregion of parameter space.

5.1.1. Step 1: Preprocessing

The input parameter space Γ is first decomposed into n_e non-overlapping rectangular elements $\{B^j\}_{j=1}^{n_e}$. In each element, B^j, a set of l points $\{q_k^j\}_{k=1}^{l}$ are chosen, and their weights $\{w_k^j\}_{k=1}^{l}$ are calculated. They correspond to a numerical integration (or quadrature) rule over the element such that:

$$\sum_{k=1}^{r} f\left(q_k^j\right) w_k^j \approx \frac{1}{\mathrm{vol}(B^j)} \int_{B^j} f(x)\mathrm{d}x \tag{20}$$

for f in a class of functions is specified by the quadrature rule. Here, the weights have been normalized so that $\sum_{k=1}^{r} w_k^j = 1$. These quadrature points will prescribe the sampling locations later in the procedure. Here, only the Smolyak sparse grid quadrature rules are considered. Fig. 16 shows the meshes of elements, i.e., subregions, as well as the sampling points with prescribed quadrature in a two-dimensional ($n = 2$) parameter space Γ.

5.1.2. Step 2: Mathematical metric

The variance is used as a mathematical metric to characterize the sensitivity of individual system outputs to chosen random inputs in each element B^j. Here, y_m represents any output of interest. Thus, $S[B^j, y_m]$ is the metric of its sensitivity to the input parameters in each element B^j, defined as:

$$\begin{aligned} S[B^j, y_m] &= \mathrm{Var}_{B^j}[y_m(x)] = E[y_m^2(x)] - E[y_m(x)]^2 \\ &= \frac{1}{\mathrm{vol}(B^j)} \int_{B^j} y_m^2(x)\mathrm{d}x - \left(\frac{1}{\mathrm{vol}(B^j)} \int_{B^j} y_m(x)\mathrm{d}x \right)^2 \\ &\approx \sum_{k=1}^{r} y_m^2\left(q_k^j\right) w_k^j - \left(\sum_{k=1}^{r} y_m\left(q_k^j\right) w_k^j \right)^2 \end{aligned} \tag{21}$$

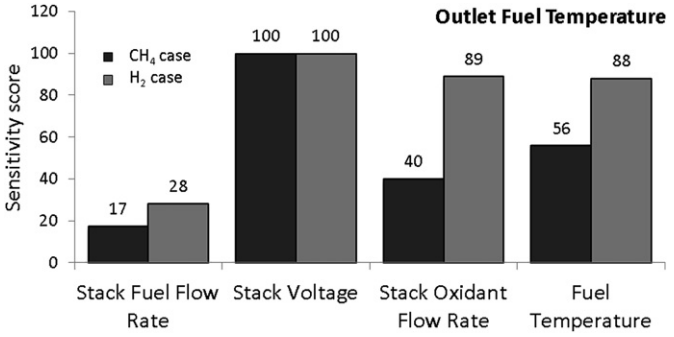

Fig. 10. Comparison of sensitivity score of input parameters between CH_4 case and H_2 case for outlet fuel temperature.

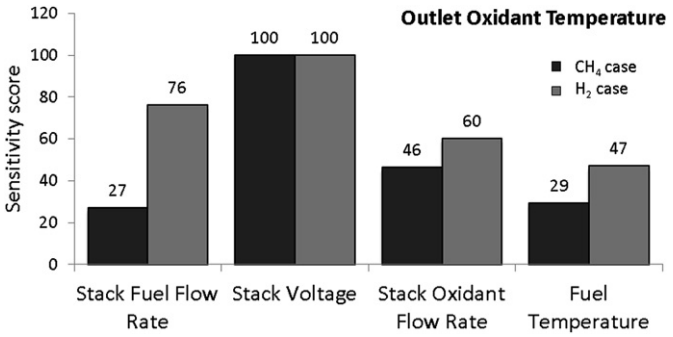

Fig. 12. Comparison of sensitivity score of input parameters between CH_4 case and H_2 case for outlet oxidant temperature.

5.2. Results

To illustrate, just as with the responsive surface calculation, we perform the analysis for two outputs: the stack current and outlet oxidant temperature. Because the stack fuel flow rate and stack voltage are the top two inputs in the rank for the selected two outputs (see Figs. 3 and 7), the analysis is conducted in the two-dimensional input space composed of these two inputs. Their range is kept as the original desired range shown in Table 1. For the other two input parameters, the stack oxidant flow rate is fixed at 0.3 mol s^{-1}, and the fuel temperature is fixed at 700 °C.

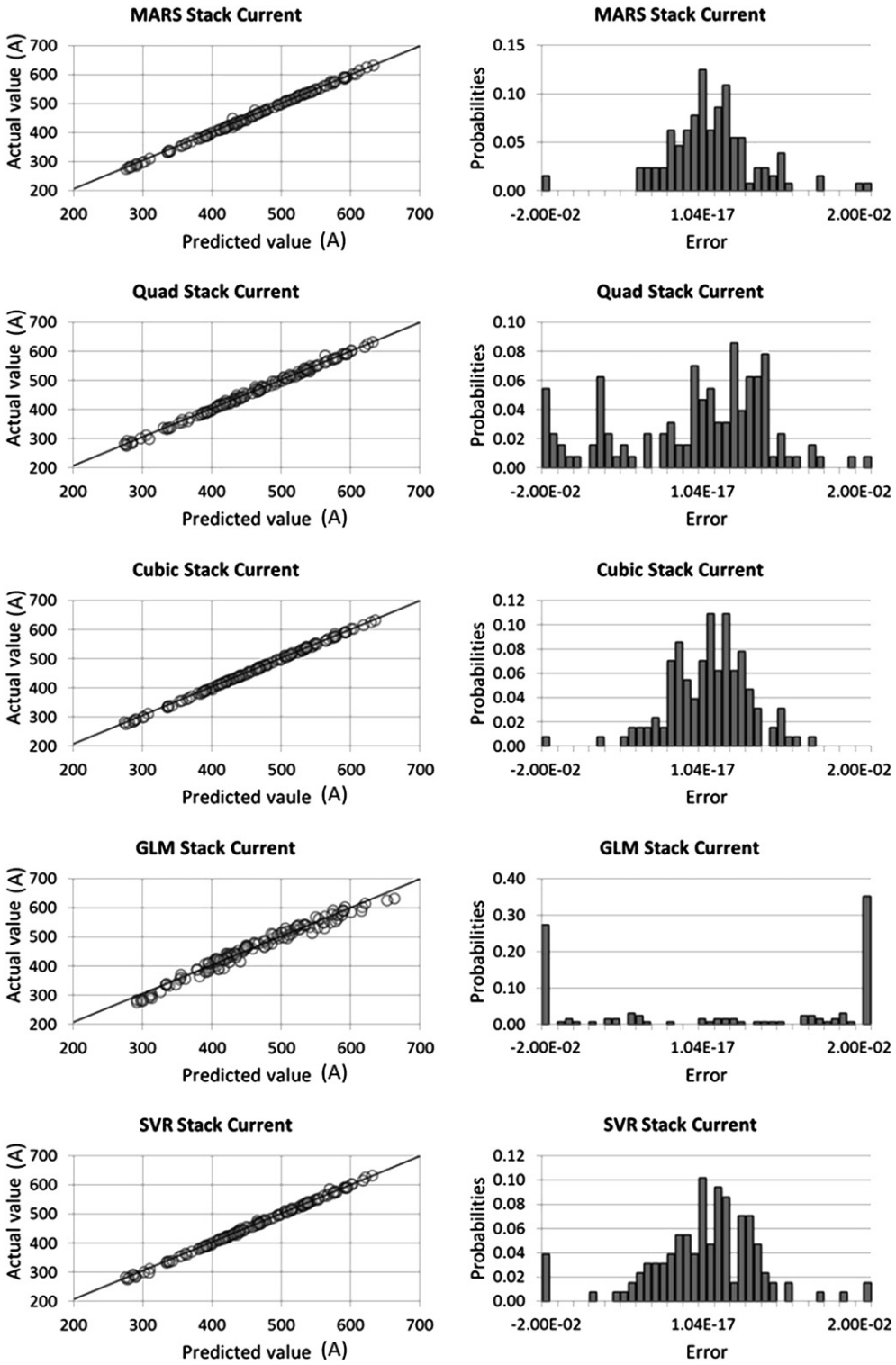

Fig. 13. Correlation between the predicted values and the actual simulation values of the stack current for different regression methods (*left column*); histogram of errors for different regression methods (*right column*).

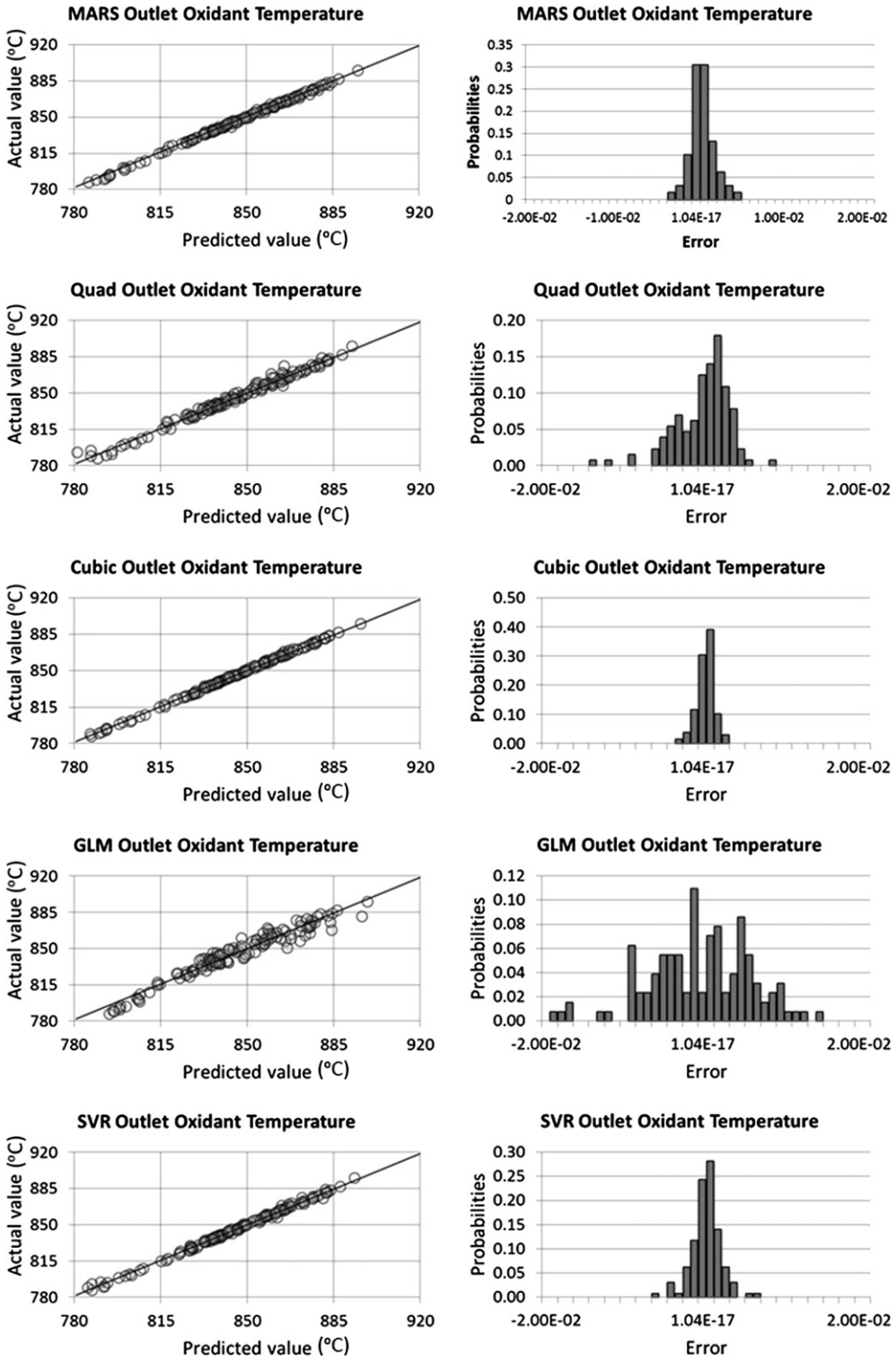

Fig. 14. Correlation between the predicted values and actual simulation values of the outlet oxidant temperature for different regression methods (*left column*); histogram of errors for different regression methods (*right column*).

Figs. 17 and 18 show the results of the sensitivity of stack current and outlet oxidant temperature, using the metric of $S[B^j, y_m]$ defined in Eq. (21) in a two-dimensional ($n = 2$) input space of stack fuel flow rate and stack voltage. From this analysis, it is noticeable that both outputs are more sensitive to the input parameters when both inputs are close to their upper limits but less sensitive to the input parameters when both inputs are close to their lower limits. This sensitivity matrix indicates that if additional sampling points are needed to augment the set and increase the responsive surface accuracy, the sampling should be biased toward this region of the parameter space.

Table 2
R-square value of each regression method for different output parameters.

	MARS	Quad	Cubic	GLM	SVR
Stack current	0.9986	0.9968	0.9993	0.9743	0.9985
Outlet cell maximum temperature	0.9980	0.9950	0.9955	0.9836	0.9949
Outlet fuel H_2 molar fraction	0.9989	0.9952	0.9991	0.9631	0.9987
Outlet fuel temperature	0.9996	0.9981	0.9998	0.9919	0.9998
Outlet oxidant temperature	0.9976	0.9850	0.9984	0.9469	0.9957

Table 3
R-square value of the response surface on the 32 × 32 grid points.

	MARS	Cubic
Stack current	0.9993	0.9995
Outlet oxidant temperature	0.9985	0.9983

6. Predicting state variables by a PCA-based mapping

Thus far, the output variables examined have singular values for the stack operating state. In addition to these global values, it also may be desirable to evaluate the actual distribution of internal variables, such as the species concentration, current density, or temperature, which are named as state variables. Their distributions are defined by the inherent resolution of the computational mesh in the chosen stack model. Performing the regression step on every single point in these distributions is not desirable and likely intractable. Therefore, we instead perform mapping from the inputs to the ranked scores of these variables using the principal component analysis (PCA). The main steps of the algorithm are reviewed as follows [49]:

(1) Implement a sampling to obtain a set of p points in the input parameter space.
(2) Run the simulations one by one with all sampled p inputs and extract the distribution of the state variable of interest on the m mesh points. Formulate a state matrix $\boldsymbol{S} \in R^{m\times p}$.
(3) Implement the singular value decomposition (SVD) on the state matrix and yield $\mathbf{S} = \mathbf{W\Sigma V^T}$.
(4) According to required accuracy and the cutoff criterion, select the reduced rank $r \ll m$.
(5) Extract the ranked principal components as $\boldsymbol{\Psi} = \boldsymbol{W}^{(r)} \in R^{m\times r}$ and scores as $\boldsymbol{\alpha} = \boldsymbol{\Sigma}^{(r)}(V^{(r)})^T$.
(6) Build the mapping from the inputs to the reduced scores $\boldsymbol{\alpha}(R^{r\times p}$ as $\boldsymbol{\alpha} = \boldsymbol{F}(\boldsymbol{x})$.
(7) Formulate the mapping for the state variable as $\boldsymbol{S} = \boldsymbol{W}^{(r)}\boldsymbol{F}(x)$, according to which, for any individual input point, the distribution of the state variable of interest on the m mesh points is predicted.

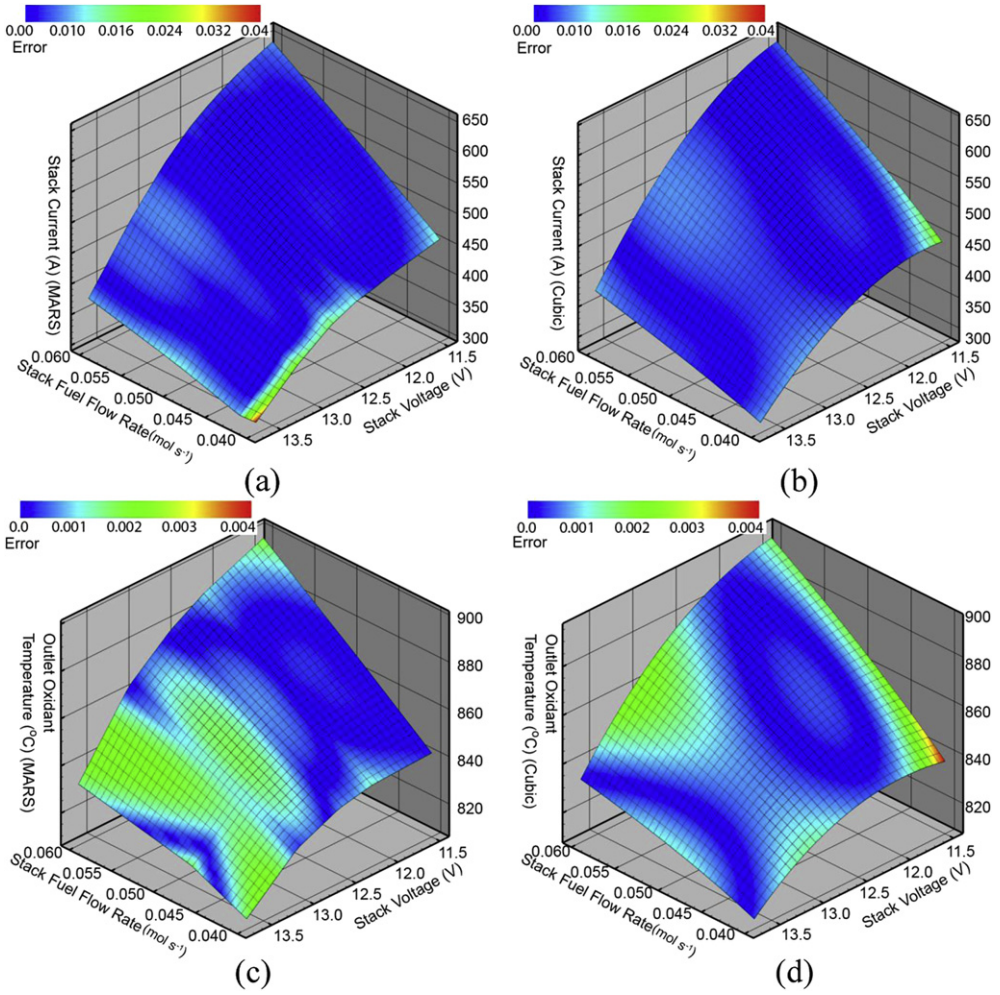

Fig. 15. Responsive surface and the absolute value of scaled error distribution, (a) MARS for stack current; (b) cubic polynomial for stack current; (c) MARS for outlet oxidant temperature; (d) cubic polynomial for outlet oxidant temperature.

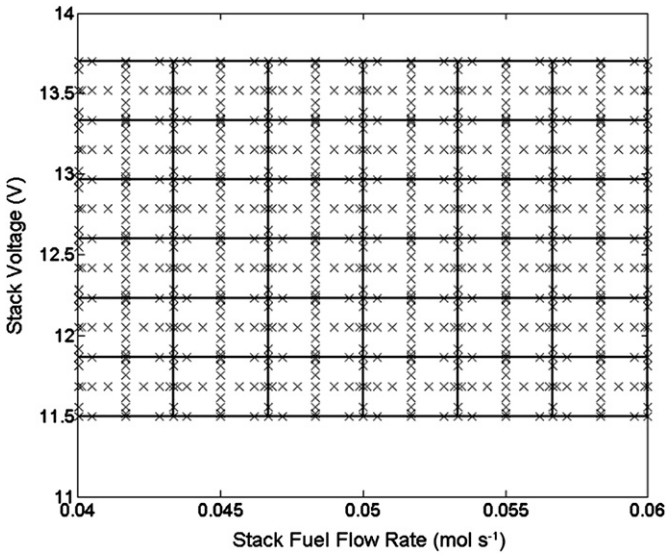

Fig. 16. Clenshaw-Curtis Smolyak sparse quadrature grids in a two-dimensional ($n = 2$) input space of stack fuel flow rate and stack voltage.

Following these steps with the 128 QMC sampling points (Section 3.2.1), the analysis is performed. On the 16th cell, the maximum temperature of the cell (variable *T_PEN*) is chosen as the state variable of interest, which has distribution on 101 mesh points. The SVD is performed on the state matrix and yields:

$$\begin{bmatrix} 101 \times 128 \\ S \end{bmatrix} = \begin{bmatrix} 101 \times 101 \\ W \end{bmatrix} \begin{bmatrix} 101 \times 128 \\ \Sigma \end{bmatrix} \begin{bmatrix} 128 \times 128 \\ V^T \end{bmatrix}. \quad (22)$$

The matrix Σ is a diagonal matrix and has only 12 non-zero values: 9.12e4, 0.14e4, 0.082e4, 0.020e4, 0.0093e4, 0.0032e4, 0.0015e4, 0.0007e4, 0.0004e4, 0.0003e4, 0.0002e4, and 0.0001e4.

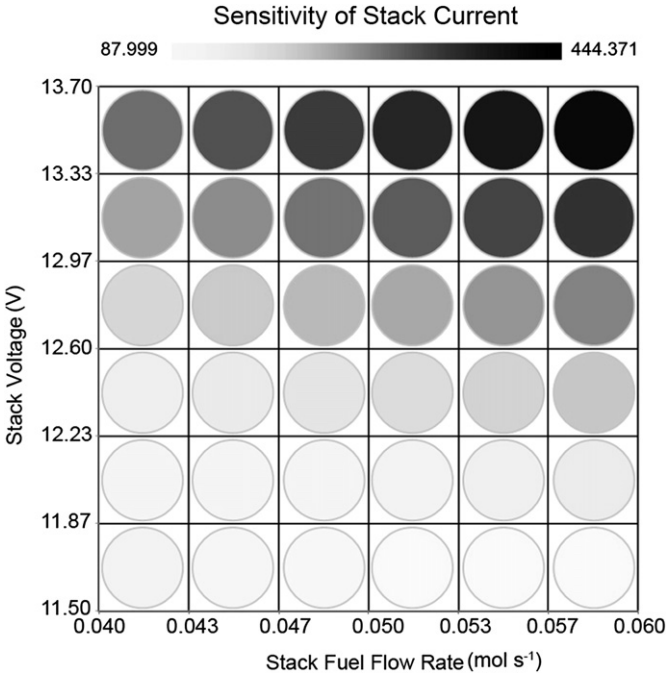

Fig. 17. Sensitivity of the stack current, i.e., $S[B^j, y_m]$ with y_m = stack current, in a two-dimensional ($n = 2$) input space of stack fuel flow rate and stack voltage.

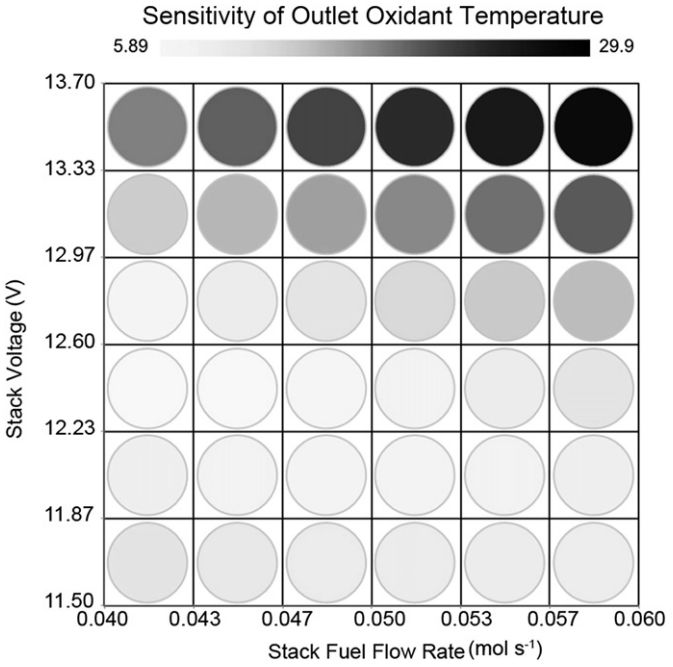

Fig. 18. Sensitivity of the outlet oxidant temperature, i.e., $S[B^j, y_m]$ with y_m = outlet oxidant temperature, in a two-dimensional ($n = 2$) input space of stack fuel flow rate and stack voltage.

If we keep all of the 12 non-zero values of Σ, i.e., $r = 12 \ll 101$, then we have:

$$\begin{bmatrix} 101 \times 128 \\ S \end{bmatrix} = \begin{bmatrix} 101 \times 12 \\ W \end{bmatrix} \begin{bmatrix} 12 \times 128 \\ \Sigma \end{bmatrix} \begin{bmatrix} 128 \times 128 \\ V^T \end{bmatrix}. \quad (23)$$

It can be reformulated as:

$$\begin{bmatrix} 101 \times 128 \\ S \end{bmatrix} = \begin{bmatrix} 101 \times 12 \\ W \end{bmatrix} \begin{bmatrix} 12 \times 128 \\ \Sigma V^T \end{bmatrix}. \quad (24)$$

Because only the first value among the 12 non-zero values is dominant in this demonstration case, r can be further reduced to 1. Then, the mapping is built from the inputs to the reduced scores, i.e., α, as in step (6). Here, the MARS and cubic polynomial regression methods are chosen to obtain the $\boldsymbol{F}(\boldsymbol{x})$.

As discussed in step (7), now if an input (not among the 128 QMC sampling points) is selected, its corresponding distribution of *T_PEN* on the 101 mesh points is able to be predicted (as illustrated in Fig. 19). It is shown that if $r = 12$ is taken, the predicted distribution agrees very well with the actual distribution. If $r = 1$ is taken, a larger

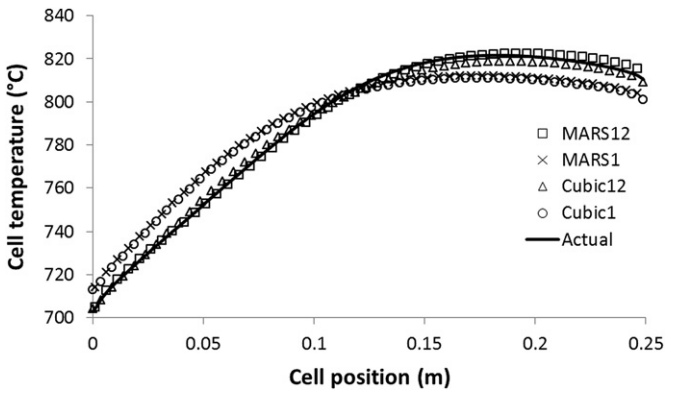

Fig. 19. Distribution of cell temperature in 16th cell in the stacked fuel cells.

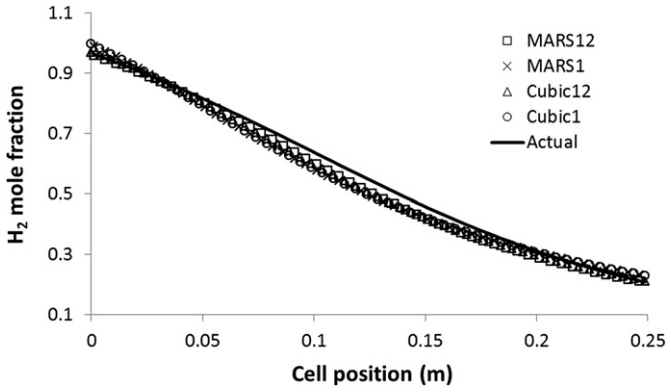

Fig. 20. Distribution of the fraction of H_2 in the 16th cell in the fuel cell stack.

error is observed. However, taking into account the computational cost saved by performing only 1 regression instead of 12 to predict the whole distribution, its performance still is notable and in practice an acceptable level of reduction can be selected. Therefore, this approach is critical in system level studies to identify maxima and minima from distributions of variables internal to the stack which are not accessible in the thermodynamic stack models used currently.

Because the temperature distributions on different components in each cell are quite similar (see Fig. 4 in Supplementary data), the fraction of H_2 (variable PH_2) in the outlet fuel composition is chosen as another example of a state variable to be analyzed, following the same described steps. Again, an input (not in the 128 QMC sampling points) is chosen, and its corresponding distribution of PH_2 on the 101 mesh points is predicted accurately, even with $r = 1$, as shown in Fig. 20.

7. Conclusions

High fidelity numerical models of fuel cell stacks and other components are needed for efficient simulations of power systems and development of controls. This work demonstrated how response surface analysis combined with sensitivity and principal component analysis could be used to develop a fast reduced order model for an SOFC stack. The developed framework creates this model for the user based on sampled inputs from an existing detailed stack model with outputs tailored to the user's needs. Automated sensitivity and error analyses are performed to ensure that sampling of the design space is sufficient to provide high accuracy of the response surfaces, and the developed framework allows the sample set to be augmented as needed to achieve the accuracy desired by the user. Principal component analysis is used to evaluate special distributions of internal stack parameters such as cell temperature that are not usually accessible in system-level stack models but are important to the fuel cell designer to prevent degradation processes. After these generation and qualification steps, this model then can be used to provide accurate information about stack performance metrics and distributions over a diverse range of operating conditions with minimal computational effort. This approach was successfully demonstrated for a multi-cell stack and will provide system modelers with a more useful stack calculator based on their existing detailed stack model.

Acknowledgments

This work was funded as part of the Solid State Energy Conversion Alliance Core Technology Program by the U.S. Department of Energy's National Energy Technology Laboratory. PNNL is operated by Battelle for the U.S. Department of Energy under Contract DE-AC05-76RL01830.

Appendix A. Supplementary material

Supplementary data associated with this article can be found, in the online version, at http://dx.doi.org/10.1016/j.jpowsour.2013.01.057.

References

[1] E.D. Wachsman, C.A. Marlowe, K.T. Lee, Energy Environ. Sci. 5 (2012) 5498–5509.
[2] NETL, Analysis of Integrated Gasification Fuel Cell Plant Configurations. DOE/NETL-2011-1482 (2011).
[3] NETL, Analysis of Natural Gas Fuel Cell Plant Configurations. DOE/NETL-2011-1486 (2011).
[4] M. Powell, K. Meinhardt, V. Sprenkle, L. Chick, G. McVay, J. Power Sources 25 (2012) 377–384.
[5] D. Hennessy, Solid oxide fuel cell diesel auxiliary power unit demonstration, in: U.S. DOE Hydrogen Fuel Cells Program 2012 Annual Merit Review Proceedings, 2012.
[6] K. Lai, B.J. Koeppel, K.S. Choi, K.P. Recknagle, X. Sun, L.A. Chick, V. Korolev, M. Khaleel, J. Power Sources 196 (2011) 3204–3222.
[7] M. Li, J.D. Power, J. Brouwer, J. Fuel Cell. Sci. Technol. 7 (2010) 041017-1.
[8] M. Li, J. Brouwer, A.D. Rao, G.S. Samuelsen, J. Power Sources 196 (2011) 5903–5912.
[9] EIA, Annual Energy Outlook 2012 with Projections to 2035. DOE/EIA-0383 (2012).
[10] J. Burkardt, Q. Du, M. Gunzburger, H.C. Lee, Reduced Order Modeling of Complex Systems, Dundee, NA03. 2003.
[11] J. Burkardt, M. Gunzburger, H. Lee, SIAM J. Sci. Comput. 28 (2006) 459–484.
[12] D.L. Damm, A.G. Fedorov, J. Power Sources 159 (2) (2006) 956–967.
[13] H. Xi, J. Sun, V. Tsourapas, J. Power Sources 165 (1) (2007) 253–266.
[14] F. Jurado, J. Power Sources 129 (20) (2004) 205–215.
[15] F. Leucht, W.G. Bessler, J. Kallo, K. Friedrich, H.M. Steinhagen, J. Power Sources 196 (3) (2011) 1205–1215.
[16] Z. Bai, P. Feldmann, R. Freund, How to make theoretically passive reduced-order models passive in practice, in: The IEEE Custom Integrated Circuits Conference (CICC), 1998.
[17] Z. Bai, R.S. Slone, W.T. Smith, Q. Ye, Comput.-Aided Des. Integrated Circuits Syst. 18 (1999) 133–141.
[18] A. Heiat, Inf. Softw. Technol. 44 (2002) 911–922.
[19] W. Lou, S. Nakai, Food Res. Int. 34 (2001) 573–579.
[20] D. Amsallem, C. Farhat, AIAA J. 46 (2008) 1803–1813.
[21] D. Amsallem, J. Cortial, C. Farhat, AIAA J. 48 (2010) 2029–2037.
[22] P.D. Allison, Am. J. Sociol. 83 (1977) 144–153.
[23] L.S. Aiken, S.G. West, Multiple Regression: Testing and Interpreting Interactions, Sage Publications Inc, Thousand Oaks, 1991.
[24] J. Ring, Am. Stat. 48 (1994) 209–213.
[25] P. McCullagh, J. Nelder, Generalized Linear Models. Boca Raton, second ed., 1989.
[26] G.E.P. Box, Ann. Math. Stat. 25 (1954) 290–302.
[27] F.J. Anscombe, J. R. Stat. Soc. Ser. A 111 (1948) 181–211.
[28] J.M. Chambers, T.J. Hastie, Statistical Models in S, Chapman and Hall/CRC, Boca Raton, 1992.
[29] J.H. Friedman, Fitting functions to noisy data in high dimensions, in: Wegman, Gantz, Miller (Eds.), Twentieth Symposium on the Interface, American Statistical Association, Alexandria, 1988.
[30] J.H. Friedman, Ann. Stat. 19 (1991) 1–141.
[31] J.H. Friedman, Stanford University, Tech. Report LCS108, 1991.
[32] J.H. Friedman, Stanford University, Tech. Report LCS110, 1993.
[33] J.H. Friedman, B.W. Silverman, Stanford University, Tech. Report SLAC-PUB-4390, 1987.
[34] P. Craven, G. Wahba, Numer. Math. 31 (1979) 317–403.
[35] A. Tarantola (Ed.), Society for Industrial and Applied Mathematics, Philadelphia, PA, USA, 2005, p. 342.
[36] Z. Hou, M.L. Rockhold, C.J. Murray, Environ. Earth Sci. 66 (2012) 2403–2415.
[37] J.W. Tukey, Exploratory Data Analysis, Addison-Wesley, Boston, 1977.
[38] Y. Benjamini, Am. Stat. 42 (1988) 257–262.
[39] P.J. Rousseeuw, I. Ruts, J.W. Tukey, Am. Stat. 53 (1999) 382–387.
[40] J.H. Friedman, Ann. Stat. 19 (1991) 1–67.
[41] H. Drucker, C.J.C. Burges, L. Kaufman, A.J. Smola, V.N. Vapnik, in: Advances in Neural Information Processing Systems 9 (NIPS), MIT, MA, 1996, pp. 155–161.
[42] A.J. Smola, B. Scholkopf, Stat. Comput. 14 (2004) 199–222.
[43] C. Tong, PSUADE User's Manual, Lawrence Livermore National Laboratory, 2009.
[44] J. Foo, X. Wan, G. Karniadakis, J. Comput. Phys. 227 (2008) 9572–9595.
[45] J. Foo, S. Sindi, G. Karniadakis, IET Syst. Biol. 3 (2009) 239–254.
[46] J. Foo, Z. Yosibash, G. Karniadakis, Comput. Methods Appl. Mech. Eng. 196 (2007) 4250–4271.
[47] R.G. Ghanem, Comput. Methods Appl. Mech. Eng. 168 (1999) 19–34.
[48] R.G. Ghanem, ASCE J. Eng. Mech. 125 (1999) 26–40.
[49] Y. Lang, A. Malacina, L.T. Biegler, S. Munteanu, J.I. Madsen, S.E. Zitney, Energy Fuels 23 (2009) 1695–1706.